Using a smartphone camera for nanosatellite attitude determination

Rogan Shimmin, Cedric Priscal, Ken Oyadomari, Watson Attai, Jasper Wolfe, Oriol Tintore Gazulla, Alberto Guillen Salas
Stinger Ghaffarian Technologies, Inc.

Abstract

The PhoneSat project at NASA Ames Research Center has repeatedly flown a commercial cellphone in space. As this project continues, additional utility is being extracted from the cell phone hardware to enable more complex missions. The camera in particular shows great potential as an instrument for position and attitude determination, but this requires complex image processing. This paper outlines progress towards that image processing capability.

Initial tests on a small collection of sample images have demonstrated the determination of a Moon vector from an image by automatic thresholding and centroiding, allowing the calibration of existing attitude control systems. Work has been undertaken on a further set of sample images towards horizon detection using a variety of techniques including thresholding, edge detection, applying a Hough transform, and circle fitting. Ultimately it is hoped this will allow calculation of an Earth vector for attitude determination and an approxmate altitude. A quick discussion of work towards using the camera as a star tracker is then presented, followed by an introduction to further applications of the camera on space missions.

1. INTRODUCTION

The ongoing PhoneSat project at NASA Ames Research Center exploits the economies of scale inherent in consumer electronics, particularly cellular phones, in order to make satellites cheaper. The fundamental requirements for a satellite architecture are all present in a cellular phone: a communications system, a power system, a high speed processor with more available memory than any other satellite launched to date, and a useful sensor suite including GPS, accelerometer, gyroscope and magnetometer.

Until recently, the phone camera was treated merely as a convenient payload initially providing photographs to stress the communications system with a high bandwidth requirement, and later demonstrating the success of the attitude control system by taking photographs of specific targets. However, the increasingly high resolution cameras available in cellphones can be used to detect state data about the spacecraft it is mounted on.

The PhoneSat 2 architecture, launched on 19 November 2013 on a Minotaur rocket and again on 18 March 2014 on an Antares rocket, used a Samsung Nexus S cellphone (i9020), with a 5MP camera as shown in Fig. 1.

(a) Samsung Nexus S

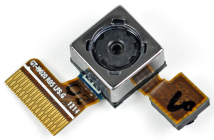

(b) Camera

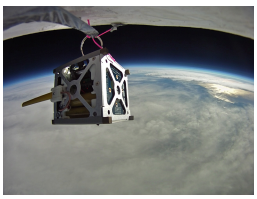

(c) PhoneSat 1.0 during high-altitude balloon test

Fig. 1

2. HORIZON DETECTION

A number of images of the limb of the Earth were randomly selected from the internet for testing, and are shown in Fig. 2. Various techniques were used to extract useful navigation data from the images, based around calculating the equation of the line that is the horizon.

First, since the background is entirely black, colour data is not necessary to identify foreground features. Consequently the hue and saturation are discarded, retaining only the luminance data. A number of techniques are available to begin separating the resulting greyscale image into segments [1, 2].

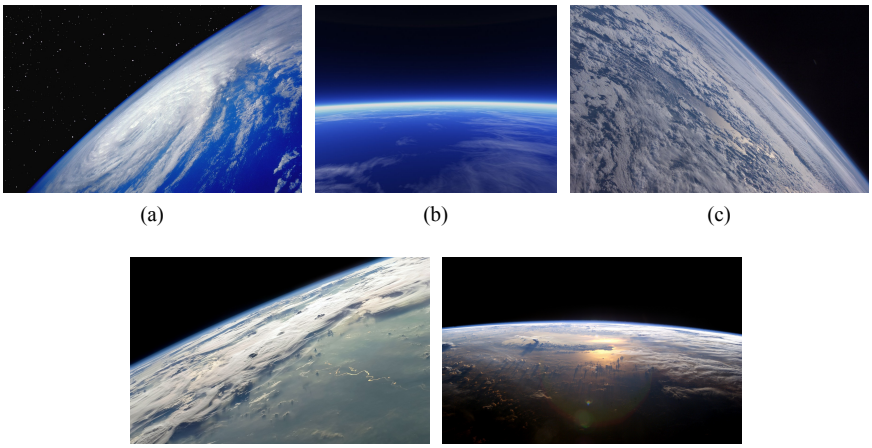

(a) (b) (c)

(d) (e)

Fig. 2. Test images used for horizon detection

2.1. THRESHOLDING

Thresholding is the simplest and most common segmentation technique, where a boolean value is assigned to each pixel based on whether its luminance is greater or less than a certain threshold. There are schemes of varying complexity to determine this threshold. Many use a histogram of the luminance values present in the image to determine one global threshold for the entire image. Intuitively, this technique should work for the above images as the darkness of space should have an obviously different luminance to the Earth. However, as seen in the test image histograms in Fig. 3 this is not necessarily the case.

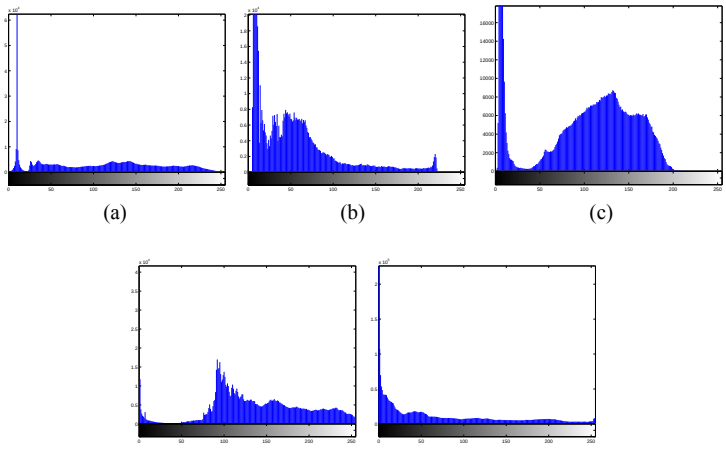

(a) (b) (c)

(d) (e)

Fig. 3. Luminance histogram for horizon detection test images. Axes are luminance vs. number of pixels with that luminance.

Each of the images exhibit a large spike at very low luminance which represents the majority of the dark “space”. In some cases this is not at zero luminance (“space” is not entirely black due to a photography artifact) but the larger problem arises from the ramp down from that spike. On most of these images that represents a colour gradient due to atmospheric blurring of the horizon. In Figs. 2a, 2c, and 2d the atmosphere is relatively thin and does not affect the outcome significantly. Fig. 2b however is presumably taken from a lower altitude because the atmosphere is visibly distorting the horizon, as seen in the noisy histogram in Fig. 3b. Some of the pixels that should be identified as “space” have a high luminance. Consequently assuming that space is dark and choosing a low threshold will not work, as

evident in Fig. 5.

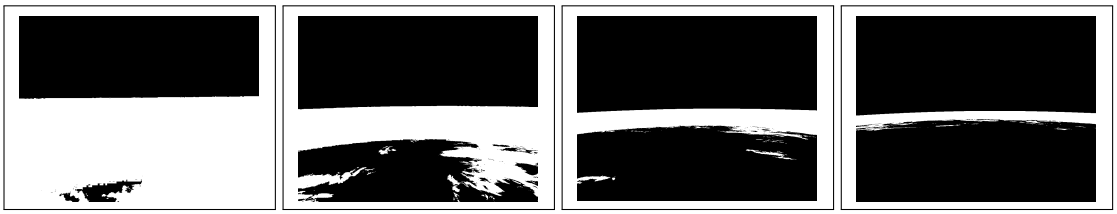

(a) Threshold=30 (b) Threshold=63 (c) Threshold=100 (d) Threshold=150

Fig. 4. Results of varying threshold values for Fig. 2b

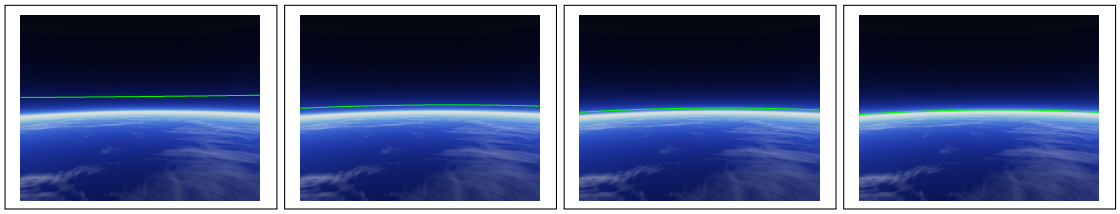

(a) Threshold=30 (b) Threshold=63 (c) Threshold=100 (d) Threshold=150

Fig. 5. Resulting horizon detected for thresholds in Fig. 4

The atmospheric scattering within Fig. 2b requires a very high threshold, which leads in to the next problem, which is also present in Fig. 2d. As seen reflected in the ocean, the Sun is just out of frame. This results in the portion of the Earth nearest the camera being heavily shadowed, resulting in the entire histogram becoming a ramp down from the peak in Fig. 3d, which means that choosing too low a threshold will not work, as evident in Fig. 5. Some pixels that should be identified as "Earth" have a very low luminance. When the "Earth" pixel luminance is low, and the "space" pixel luminance is high, there may be no global threshold that would segment the image correctly, so another technique must be used.

Some shortcomings of this method may be overcome with further processing. The stars evident in Fig. 10a may be removed morphologically, by removing any cluster below a certain number of pixels. The dark shadowed patches on the Earth may subsequently be removed the same way, by inverting the image and performing the same operation. Since only two large clusters are expected (space and the Earth) the morphological limit may be set high, which yields a nicely segmented Earth/space image, as seen in Fig. 6b. Setting the threshold higher avoids shadowing on the horizon, and setting the black morphological cluster limit higher eliminates the shadow nearest the camera (or in this case, viewer, as visible stars indicates that this may be an artificial image).

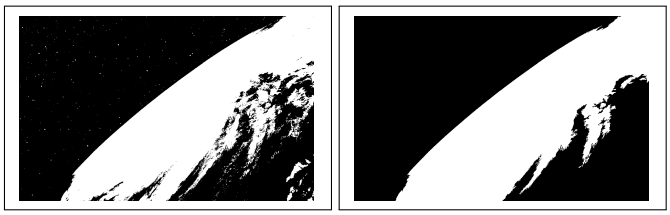

(a) Unprocessed thresholded image (b) Filtered thresholded image

Fig. 6. Highlighting the necessity for additional image filtering resulting from Fig. 2a

As seen in Fig. 4 the threshold is sometimes driven very high by atmospheric scattering. This can result in large shadowed portions of the Earth. Subsequently the limits on morphological processing should differ depending on the scenario: if a high threshold is required, then the black morphological cluster limit should also be higher, while the

white cluster limit should be lower. Trial and error on the test images indicated that a suitable limit for the black clusters is half of the number of black pixels after thresholding. This should be a foolproof limit provided the image is close to half Earth, half space. Less critical is the limit for the white clusters, but that was found optimal at about one eighth of the number of white pixels after thesholding.

However, even this technique runs into difficulty on Fig. 2e. If the threshold is too low, atmospheric scattering distorts the horizon significantly as seen in Fig. 7a. As the threshold is raised, the shadowed portions of the Earth grow. The problem arises when the shadowed portion of the Earth becomes larger than the "space" background before the threshold is high enough to exclude atmospheric scattering. Consequently, morphological processing will fill in "space" and try to find a horizon within the shadow, as seen in Fig. Fig. 7.

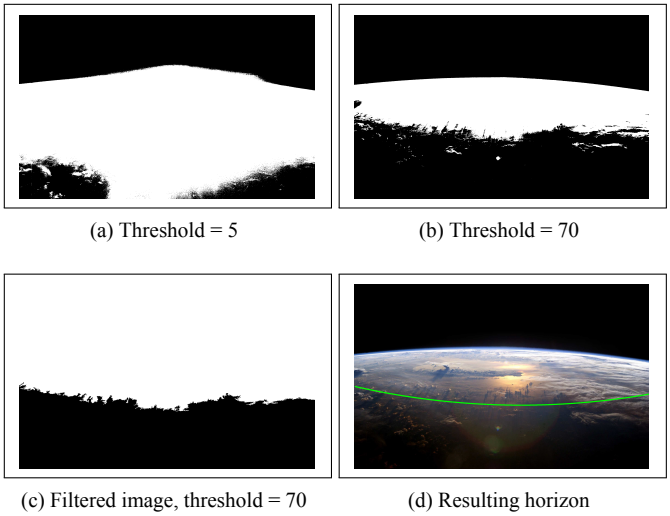

(a) Threshold = 5 (b) Threshold = 70

(c) Filtered image, threshold = 70 (d) Resulting horizon

Fig. 7

In these scenarios a more intelligent approach is required. One of the most common alternative approaches to thresholding is clustering.

2.2. CLUSTERING

Clustering is the process of categorising data points based on some relationship between them. The most common clustering technique for images is known as *k-means clustering*. This involves picking k starting data points, and then assigning all remaining data points to one of the original k points to minimise that relationship, often known as the "distance". The k seed points are then reassigned to the centroid of their respective clusters, and the procedure is repeated, until the centroids no longer move (within some defined tolerance).

In this scenario, the obvious relationship is the image luminance. However, even if you could guarantee that only one seed point was within each desired segment (the Earth, and space) this technique devolves to an automatic, global thresholding. The heuristic may of course be adapted to the scenario: one obvious modification would take some weighted average of luminance with actual distance between the pixels, on the assumption that pixels representing the Earth are physically close together, and pixels representing space are close together. However, the horizon remains a problem, being equidistant between the two centroids and also a region of blurred luminance as seen in Fig. 2b.

There are clustering schemes to autonomously generate a threshold such as Otsu's method[3], the Balanced Histogram Thresholding Method[4], and the Iterative Selection Thresholding Method[5]. Each of these algorithms has its own advantages and flaws depending on the image in question, which may lead to unexpected behaviour depending on the image captured by the satellite. For example, Balanced Histogram Thresholding is heavily biased by any sequence of zeros in the histogram, especially at the extremities such as the higher order in Fig. 3c.

2.3. REGION GROWING METHODS

A technique closely related to clustering is called region growing. The primary difference is the order of pixel classification: clustering assigns all pixels to one of the centroids in each iteration, then adjusts the centroids, while region growing analyses only the pixels adjacent to each cluster. This results in the position of each pixel being much more dominant in the selection, perfect for this scenario where the only cluster of interest (the Earth) is known to be one contiguous body. The problem of selecting seed points can be easily solved by taking the four corners of the image, at least one of which must be space thanks to the circular image target. A tolerance can then be applied to merge adjacent clusters of space, or Earth.

Blurred horizons such as Fig. 2b still pose a difficulty though. The pixels bordering the cluster are compared to the mean intensity of the entire cluster. Due to the shadowed Earth in the foreground, the threshold will become low for the Earth cluster. Consequently much of the atmosphere that should be classified as “space” will be assigned to the Earth cluster. One modification that may overcome this difficulty is a localised region-growing; that is, comparing each new pixel to the mean of its adjacent pixels, and assigning it to the cluster of the most similar adjoining pixel that meets the tolerance.

2.4. EDGE DETECTION

An alternative to thresholding methods based on the first-order image luminance is to differentiate the image data and threshold based on the second-order rate of change in the luminance[6]. Fig. 8 shows the test figures after edge detection using the Sobel method[7]. However, a threshold must still be chosen within the resulting gradient data, and all of the problems with thresholding exist within this technique.

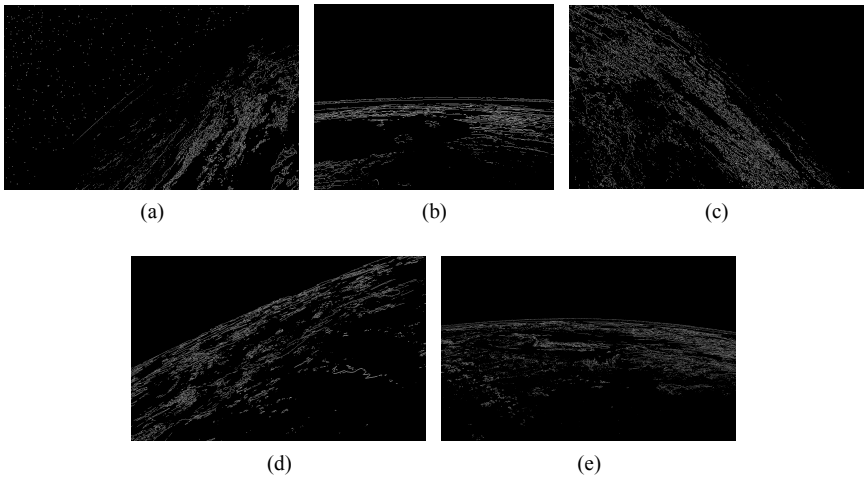

Fig. 8. Edges detected using the Sobel method

However, again this method is vulnerable to various photographic effects. The horizon is not always the brightest edge, as demonstrated by the river and the cloud line visible in Fig. 8d. Shadowing from the clouds in Fig. 2c also causes problems, as seen in Fig. 8. A common photography artifact called lens flare, seen in the bottom centre of Fig. 2e, can also interfere with the algorithm. The atmospheric blurring of the horizon seen in Fig. 2b is fortunately not a serious problem using this technique, as the colour gradient is very gentle allowing a well defined horizon visible in Fig. 8b.

2.5. BOUNDARY DETECTION

A more successful second order technique is boundary detection. Boundary detection uses an edge detection but for enclosed shapes only. Thus, like edge detection it is still very sensitive to thresholding, but the theshold can be set lower as small blobs can be discarded. Fig. 9 shows boundary detection run on the test images using the Moore-Neighbor tracing algorithm modified by Jacob's stopping criteria[8].

Atmospheric distortion has caused some offset from the actual horizon in Fig. 9b, but less than most other techniques, and in the other images the horizon is detected very effectively. The background stars in Fig. 9a, a problem that may recur with noisy pixels or single particle events on the sensor, but these should be easily morphologically filtered out. The borders along the edge of the image can be removed by cropping a single row of pixels from around the image, which just leaves the shadowed portions of the Earth that complete the enclosed boundary in Figs. 9b, 9c and 9e.

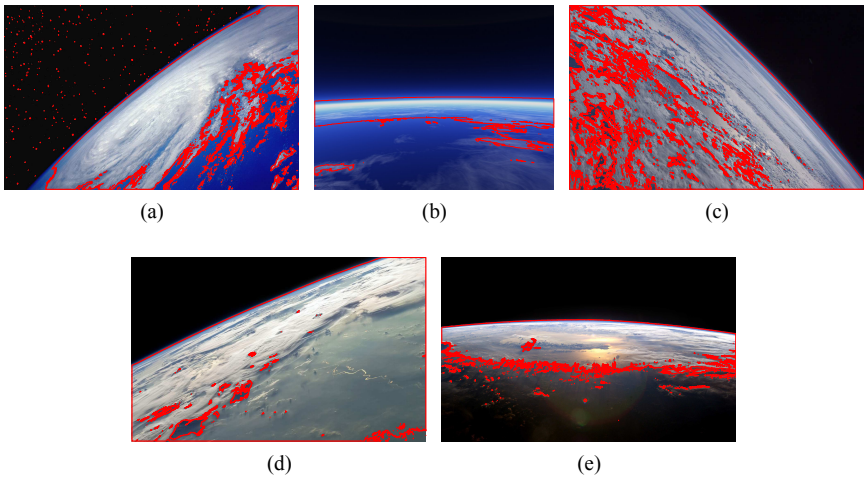

(a) (b) (c)

(d) (e)

Fig. 9. Boundaries detected using the Sobel method

2.6. HOUGH TRANSFORM

A much more versatile and robust processing technique for this scenario would be the Hough transform. The Hough transform is designed to detect circles in an image. It does this by essentially examining each pixel sequentially, and incrementing a counter for every possible circle in the image (within defined size limits) that this pixel would be part of. This technique is very effective at looking for small circles, but as the Earth is likely to be larger than the frame size there is a vast range of possible circle sizes and positions relative to the camera. Consequently the memory and processing time required for this technique rapidly expands beyond the capability even of the smartphone platform.

The memory requirements, M, may be calculated:

$$M = (W + 2 \times R_{max}) \times (H + 2 \times R_{max}) \times R_{num} \tag{1}$$

where W and H are the width and height of the image in pixels, R_{max} is the maximum radius of circles to be detected, and R_{num} is the total number of different circle radii to be searched[9]. Thus the computational complexity may be reduced by drastically downsampling the images, and correspondingly shrinking the radii of circles being searched for (a good approximation may be made based on the anticipated altitude of the spacecraft orbit) but testing on sample images did not even come close to finding the partial circle of the Earth's horizon.

2.7. OBJECTIVE

Manual threshold selection was applied based on the histograms in Fig. 3 and filtered as described previously, resulting in the segmented images shown in Fig. 10. Edge detection algorithms were then applied to the clean images. As there was no remaining noise in the image the data points were passed to a circle-fitting algorithm. The resulting circles are overlaid on the original images in Fig. 11. If a process can be established to reliably generate clean segmented images like those in Fig. 10, the fitted circles can be used to establish information about the position and distance of the Earth (or other celestial body).

The image size and field-of-view of the camera are hardware dependent, and may be defined in flight code (specifications for the Nexus S are presented in Table 1. The ratio of image size to field-of-view may then be multiplied by the centrepoint of the circle offset from the centre of the image to get an approximate Earth vector, and the altitude

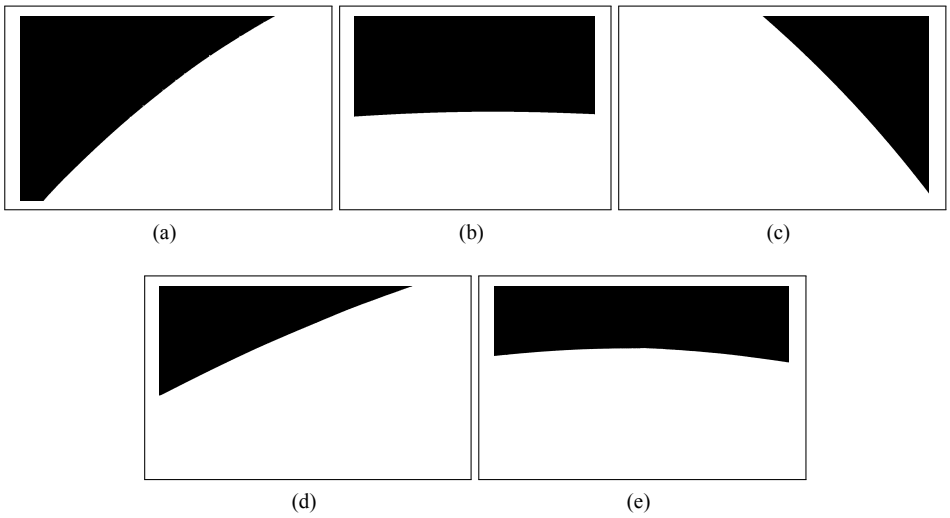

Fig. 10. Manually thresholded and automatically filtered test images for horizon detection

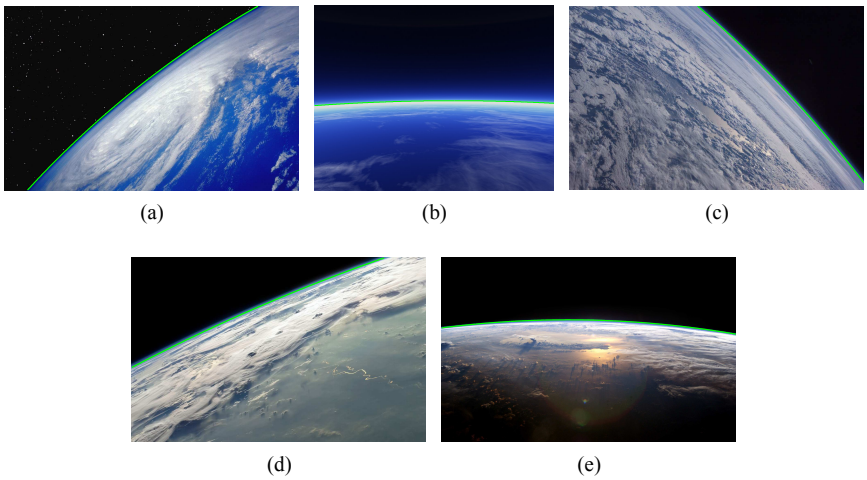

Fig. 11. Horizon line calculated by horizon detection algorithm

may be approximated based on the radius of curvature. However, this technique falls subject to the small-angle approximation[10], as demonstrated by the image field of view in Fig. 12.

Fortunately, extensive work has been undertaken within the field of machine vision to map the two-dimensional image plane to a three-dimensional spherical reference[11]. First the camera must be calibrated using known test images, to correctly model any imperfections of the particular sensor array and lens. Then a series of transformations are applied: an image translation to adjust the origin from the top left corner to the camera boresight (at the center of the image), followed by transforming the units from pixels to a real-world dimension based on intrinsic camera parameters; a perspective projection to transform the 2D position to a 3D position on the focal plane; and finally a transformation to real-world coordinates based on extrinsic camera parameters. There are many techniques for determining these transformations, including the Roger Tsai algorithm[12] and Zhang's “flexible new technique for camera calibration”[13].

Table 1. Specifications of the Nexus S camera

Device	Samsung Nexus S
Resolution	2608 x 1960
Focal length	3.63mm
f-number	2.8
Field of View (diagonal)	68°
Crop factor	9.5
Field of View	57 x 44°

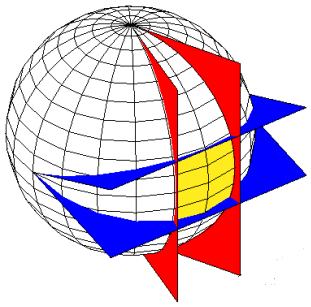

Fig. 12. Field-of-view of a square sensor array

3. MOON VECTOR DETECTION

While the Earth fills a large portion of the field of view in low Earth orbit, there are other bodies that can be used to determine attitude information. In a similar manner to the horizon detection investigation, a number of images of the Moon were randomly selected from the internet for testing, and are shown in Fig. 13. These images were taken from the Earth's surface, and subsequently include atmospheric noise and in some cases an illuminated horizon. This represents a much worse case than would be observed from orbit, assuming the pointing algorithm requires the Earth's limb and the Sun to be outside of the field of view. Nonetheless, due to the higher luminance of the Moon the algorithm was found to be far more robust than that for horizon detection.

(a) (b) (c) (d)

Fig. 13. Test images used for moon vector detection

These images were globally thresholded at a luminance of 240 (out of 255). This was possible because the Moon is so much brighter than any noise, ocean reflection or cloud refraction in the image. Figs. 13b and 13d were particularly robust, successfully detecting the centroid for a very wide range of luminance thresholds. Some lessons can be learnt from this in regards to the image acquisition: a narrow field of view works better as in Fig. 13b, and reflections off the ocean in particular should be avoided (this should not be a problem in orbit!).

Some noise was still observed in the thresholded images due to light scattering through clouds and reflections on the ocean. This was filtered out by discarding outlier points (points furthest from the centroid of the image) using the Thompson Tau method[14].

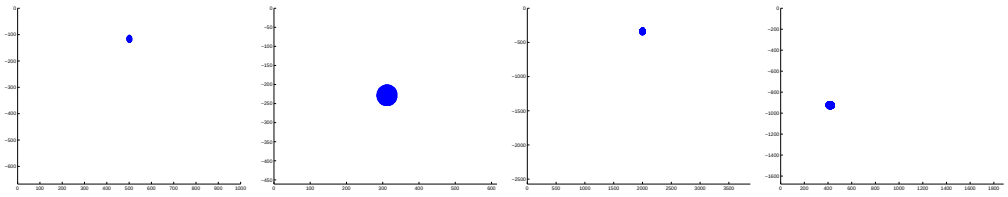

(a) (b) (c) (d)

Fig. 14. Thresholded and filtered Moon images

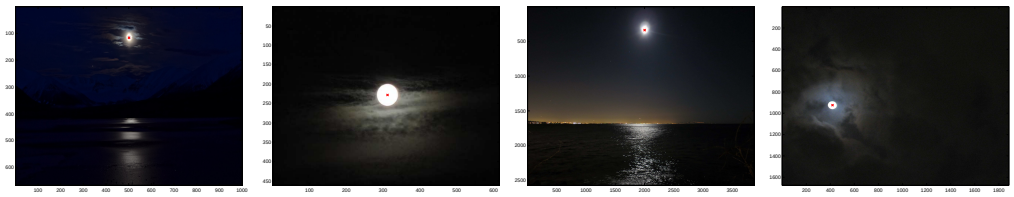

(a) (b) (c) (d)

Fig. 15. Calculated Moon centroid

3.1. OBJECTIVE

The PhoneSat ADCS is able to calculate a Moon vector based on its estimated attitude and known position and time. Aligning the satellite camera along this vector, taking a photo and processing using the algorithm outlined above to calculate the difference between the expected Moon vector and the observed Moon vector allows a quaternion offset to be applied to the ADCS, effectively calibrating the attitude.

4. STAR TRACKER

Low-cost star trackers based on commercially available cameras are being developed around the world for the burgeoning cubesat market[15]. To exploit this emerging technology, an analysis of modern smartphone cameras was undertaken within the PhoneSat program, followed by implementation of a star pattern recognition algorithm[16].

The camera investigation found that the Nexus S camera does not possess sufficient ISO sensitivity to register even the brightest stars at night. However, this work was continued using sample images taken from other smartphone cameras, and test images taken from the Stellarium planetarium software. It may be useful in a later version of PhoneSat with an updated smartphone.

The test images were analysed against a standard data set taken from the Hipparcos star catalogue[17]. The number of catalogue images required depended upon the camera field of view as shown in Table 2; the minimum number of images required to cover the celestial sphere were selected using the "covering method". Test images were translated and rotated to align the three brightest stars with each test image. The similarity between the images was then evaluated using the "shortest distance" method[18]. This essentially iterates through each catalogue star within the field of view, and assigns it a score based on how close the nearest star in the camera image is. Thus, if the catalogue star is visible in the camera image, it receives a score of zero.

Table 2. Number of catalogue images required to cover the celestial sphere

Field of view (degrees)	5	10	20	30	40	50
Number of pictures required	5185	1297	325	145	82	52

A rotation matrix is then derived from the image with the best score to determine the attitude of the spacecraft relative to the celestial sphere. This technique was found to be successful up to 95% of the time, as seen in the results in Table 3, producing an absolute accuracy of $0.18° \pm 0.04°$. Most of this error was found in right ascension ($-0.2° \pm 0.08°$)

(a) Catalogue image

(b) Isolines generated from catalogue image

Fig. 16. The generation of isolines from a catalogue image

rather than declination ($0.01° \pm 0.04°$), although it was noted that the right ascension errors mostly occurred close to the singularity when declination approaches $\pm 90°$.

However, this technique was also found to be computationally slow, as a distance must be calculated for each star in each catalogue image. Real-time performance was improved by pre-processing and calculating the distance to the nearest star for each pixel in the catalogue images ("isolines", as seen in Fig. 16).

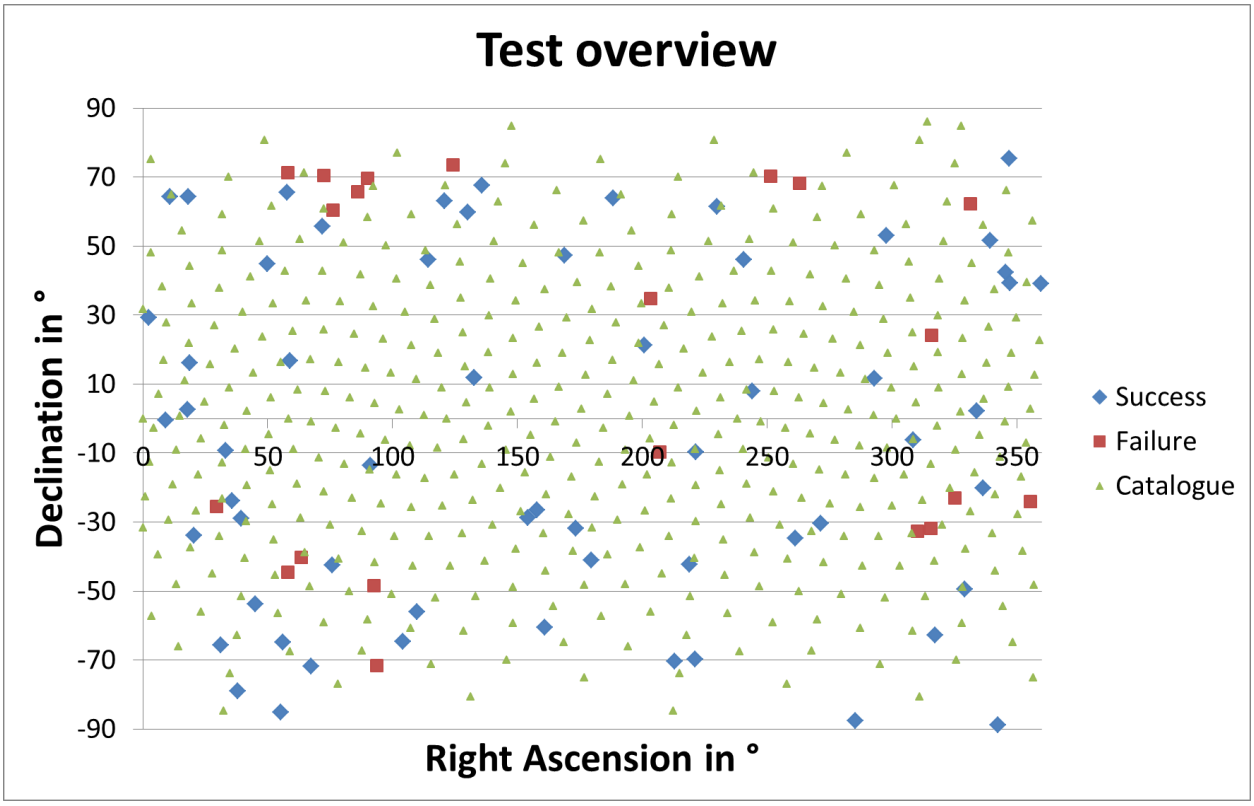

Fig. 17. Star tracker results

Table 3. Star tracker test results

Pictures in catalogue	435	1332	8192
Successes	61	61	61
Failures	21	6	3
Success rate	74.4%	91.0%	95.3%

5. LIMITATIONS

These investigations have all suffered from a variety of assumptions which must be alleviated prior to deployment as an autonomous navigation system, primarily in the selection of test images. All of these investigations have relied upon test images found on the web.

The Phonesat mission has taken images of the Earth's limb from orbit but downlink bandwidth severely impaired the available resolution. Further images will be taken on upcoming missions allowing more realistic testing. This will reduce some photography artifacts impeding the current investigation such as clouds and ocean reflecting light in the Moon detection, and some of the atmospheric scattering in the horizon detection. However the full extent of the image quality is to be determined; other artifacts may cause problems such as motion blurring, sensor blooming, and lens flare as seen in Fig. 2d.

Sensor blooming is a property of CCD (charge-coupled device) sensors, individual pixels of which may saturate and spill over into adjacent pixels. This artifact may be avoided by the use of CMOS (complementary metal oxide semiconductor) sensors. However, by nature of their design both types of sensors may still act as a diffraction grating and produce lens flare if bright lights are present in the image, or just out of the frame. Careful camera selection may help in avoiding this phemonemon, as the Apple iPhone 5 camera was particularly vulnerable to this sort of lens flare but the Apple iPhone 4S and Samsung Galaxy SIII handle it very well[19].

Lens flare may also be avoided by placing constraints on the satellite's predicted attitude when the image is taken, to ensure all bright objects except the intended subject are out of frame by at least 10 degrees (the angle may be refined by further testing). This constraint will be important regardless of lens flare, as all of the image processing techniques described above will fail if the Earth, Moon or Sun appear in an image unexpectedly.

An additional limitation of the Moon detection algorithm described here is that all of the test images featured a full Moon. Obviously this will only be a realistic approximation for a handful of days each month. As the Moon is expected to be much smaller than the Earth, the Hough transform could be more efficiently implemented to this problem than to horizon detection, allowing even incomplete circles to be detected.

6. CONCLUSION

Progress has been made towards developing an automatic attitude determination system based upon images collected by a smartphone camera. Several techniques demonstrate promise for autonomous horizon detection, although no one technique works flawlessly. In particular, localised thresholding or more specifically a localised clustering algorithm could work well in determining an Earth vector, perhaps in combination with a boundary detection algorithm to circumvent atmospheric blurring. The present Moon vector determination appears to work well. These techniques could assist with attitude determination and control calibration.

A more general purpose use for optical navigation has been attempted with the star tracker. This would allow complete attitude determination even beyond Earth orbit, greatly assisting in satellite control. The technique developed was found to be accurate down to typically 0.2° when sufficient bright stars are identified. The number of bright stars identified may be improved by increasing the search depth of the star catalogue at the expense of processing time.

All of these investigations have relied upon test images found on the internet. Results will be improved in future as further PhoneSat missions provide realistic cellphone images taken from orbit. Furthermore additional pointing constraints will have to be implemented for fully autonomous navigation to ensure useful photographs are taken.

REFERENCES

[1] M. Sezgin and B Sankur (2004) "Survey over image thresholding techniques and quantitative performance evaluation" in *Journal of Electronic Imaging*, **13**(1) pp. 146–165. DOI: 10.1117/1.1631315

[2] A Miranda Neto, A Corrêa Victorino, I Fantoni and DE Zampieri (2011) "Robust Horizon Finding Algorithm for Real-Time Autonomous Navigation Based on Monocular Vision" in *14th International IEEE Conference on Intelligent Transportation Systems*, pp. 532-537. DOI: 10.1109/ITSC.2011.6082835

[3] N Otsu (1979) "A threshold selection method from gray-level histograms" in *IEEE Transactions on System, Man, and Cybernetics*, **9**(1) pp. 62-66. DOI: 10.1109/TSMC.1979.4310076

[4] A Anjos and H Shahbazkia (2008) "Bi-Level Image Thresholding - A Fast Method" in *Biosignals*, **2** pp. 70-76.

[5] TW Ridler and S Calvard (1978) "Picture thresholding using an iterative selection method" in *IEEE Transactions on System, Man and Cybernetics*, **8**(8) pp. 630-632. DOI: 10.1109/TSMC.1978.4310039

[6] J Canny (1986) "A Computational Approach to Edge Detection" in *IEEE Transactions on Pattern Analysis and Machine Intelligence*, **8**(6) pp. 679-698. DOI: 10.1109/TPAMI.1986.4767851

[7] Mathworks (2014) *MATLAB and C/C++: The Perfect Combination for Signal Processing Algorithms* presented on Thursday 16 January 2014, Santa Clara Marriott, CA, USA.

[8] RC Gonzalez, RE Woods and SL Eddins (2004) *Digital Image Processing Using MATLAB*, Pearson Prentice Hall, New Jersey.

[9] HK Yuen, J Princen, J Illingworth and J Kittler (1989) "A Comparitive Study of Hough Transform Methods for Circle Finding" in *Proceedings of the Alvey Vision Conference*, **5**(29) pp. 1-6. DOI: 10.5244/C.3.29

[10] M Boas (2006) *Mathematical Methods in the Physical Sciences*, Wiley, New Jersey.

[11] YC Shiu and S Ahmad (1989) "3D Location of Circular and Spherical Features by Monocular Model-Based Vision" in *IEEE International Conference on Systems, Man and Cybernetics*, **2** pp. 576-581. DOI: 10.1109/ICSMC.1989.71362

[12] R Tsai (1987) "A Versatile Camera Calibration Technique for High Accuracy 3D Machine Vision Metrology Using Off the Shelf Cameras and Lenses" in *IEEE Journal of Robotics and Automation*, **3**(4) pp. 323-346. DOI: 10.1109/JRA.1987.1087109

[13] Z Zhang (2000) "A flexible new technique for camera calibration" in *IEEE Transactions on Pattern Analysis and Machine Intelligence*, **22**(11) pp. 1330-1334. DOI: 10.1109/34.888718

[14] WR Thompson (1935) "On a criterion for the rejection of observations and the distribution of the ratio of deviation to sample standard deviation" in *The Annals of Mathematical Statistics*, **6**(4) pp. 214–219. DOI: 10.1214/aoms/1177732567

[15] SA Rawshdeh, JE Lumpp, J Barrington-Brown, M Pastena (2012) "A Stellar Gyroscope for Small Satellite Attitude Determination" in *26th Annual AIAA/USU Conference on Small Satellites*, Logan, Utah, USA.

[16] F Deconinck (2013) "A smartphone based star tracker" in *International Astronautical Congress*, Beijing, China IAC-13.B4.6B.10.

[17] C Turon, M Creze, D Egret, A Gomez, M Grenon, H Jahreiß, Y Requieme, AN Argue, A Bec-Borsenberger, J Dommanget, MO Mennessier, F Arenou, M Chareton, F Crifo, JC Mermilliod, D Morin, B Nicolet, O Nys, L Prevot, M Rousseau, MAC Perryman, et al. (1993) "HIPPARCOS Input Catalogue" in *Bulletin d'information du Centre de Données Astronomiques de Strasbourg*. URL: `http://cdsarc.u-strasbg.fr/viz-bin/Cat?I/239` checked 20 August 2014.

[18] LE Sharpe (1970) *Spacecraft star trackers*, NASA SP-8026. URL: `http://hdl.handle.net/2060/19700029405` checked 18 August 2014.

[19] D Poeter (2012) “Apple Addresses iPhone 5 Lens Flare Issue” in *PCmag*, Oct 7 2012. URL: http://www.pcmag.com/article2/0,2817,2410679,00.asp checked 13 August 2014.